TERRAIN NORMALIZATION OF AVIRIS AND HYPERION IMAGERY IN FORESTED LANDSCAPES

Philip A. Townsend and Jane R. Foster[1]

1. INTRODUCTION

The effects of topographic shadowing in satellite and aerial imagery can be substantial in rugged landscapes with steep hills or mountains. These effects can affect interpretations and quantitative analyses of imagery, and in forested areas can complicate the classification of forest types or the extraction of biophysical parameters from the reflectance data. Because of this, numerous techniques have been devised to correct for terrain illumination differences, including the simple cosine (or Lambertian) correction, the Minnaert correction (Minnaert, 1941), and a variety of other approaches (e.g., Civco, 1989; Conese et al., 1993; Meyer et al., 1993). The purpose of this study is to demonstrate the application of one technique, the empirical approach of Meyer et al. (1993) to high altitude AVIRIS and Hyperion imagery. Previous work by Martin et al. (1999) compared the application of two techniques – the Lambertian (simple cosine) and Minnaert corrections – on AVIRIS, finding superior performance by the Minnaert correction. Neither of these approaches is used here, as the cosine correction is generally recognized to over-correct on shaded slopes, while the Minnaert correction requires the derivation of a cover-type specific correction coefficient, which is especially difficult when cover types are either not known or not mapped (see Allen, 2000). The empirical approach also has the benefit of providing several tools (described below) for the quantitative evaluation of the correction.

2. STUDY AREA AND METHODS

2.1 Study Area

The study area is the 15,700 ha Green Ridge State Forest (GRSF) in western Maryland (Figure 1). GRSF is located in the Ridge and Valley physiographic province of the central Appalachian Mountains, and is characterized by steep southwest-northeast trending mountains with gently sloping to steeply incised valley bottoms. Elevation ranges from 250-700 m. The forests are comprised largely of deciduous oaks, with Virginia pine on some west-facing slopes and hemlock in some valley bottoms. This research was undertaken as a component of a larger project to compare multiple sensor combinations for mapping and modeling forest composition and structure.

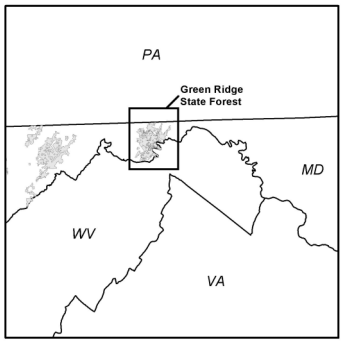

Figure 1. Location of Green Ridge State Forest in western Maryland.

Table 1. Image Characteristics

Sensor	Date	Time (UTC)	Solar Azimuth	Solar Elevation
AVIRIS	5/14/2000	15:42:46	133.8	62.62
AVIRIS	7/13/2001	15:47:47	134.94	66.72
Hyperion	7/24/2001	16:09:30	126.35	61.13

2.2 Image Preprocessing

The research presented here uses two AVIRIS images, acquired on 14 May 2000 and 13 July 2001 from an altitude of ~19,900 m, and one EO-1 Hyperion image acquired on 24 July 2001 (Table 1). The images were atmospherically corrected using the ATmospheric REMoval program (ATREM) (Gao et al., 1993) followed by an empirical line calibration (e.g., Moran et al., 2001) developed from measurements taken by an Analytical Spectral Devices (ASD) FieldSpec spectroradiometer. The AVIRIS imagery exhibited a cross-track view-angle dependent brightness gradient. This gradient of increasing brightness on the west side of the images results from the AVIRIS

[1] University of Maryland Center for Environmental Science, Appalachian Laboratory, Frostburg, Maryland 21532; townsend@al.umces.edu

scan angle and direction, flight path orientation and solar azimuth, and was corrected by fitting a first-order additive quadric curve to the mean radiance by view angle (Kennedy et al., 1997). The images were georeferenced to UTM coordinates using a triangulation method with > 70 GCPs per scene and nearest neighbor resampling.

2.3 Terrain Normalization

All of the images used in this research exhibited substantial terrain effects (Figure 2). To determine the effects of differential illumination, we modeled solar illumination for each image using slope and aspect derived from a digital elevation model (DEM) and solar altitude and azimuth information for the time of imaging (Table 1). The incidence angle of solar radiation is defined as *cos(i)*, i.e. the angle between the normal to the surface and the source of light (the sun). A linear model was then constructed to predict reflectance (on a pixel-by-pixel basis) as a function of illumination (Figure 2). The influence of illumination was then removed through detrending based on the slope of the regression equation. In general, the approach removes the slope between reflectance and illumination, while the variance in reflectance at any given incidence angle remains unchanged. The approach assumes that illumination differences are constant among cover classes (Allen, 2000). However, the training pixels used to determine the regression equation (i.e., Figure 3) are sampled from sites with similar canopy composition. For this research, the regression equations were developed using reflectance data from leafed-out mature oak forests, the dominant cover type in the region. Following Meyer et al. (1993), reflectance on the normalized image is then computed as:

$$L_H = L_T - cos(i)\, m - b + L_\mu + e \qquad \text{(Equation 1)},$$

where L_H is the normalized reflectance, L_T is the observed reflectance on sloped terrain, L_μ is the mean L_T for a channel, m is the slope and b is the y-intercept of the linear regression model; e represents model error. This regression-based approach allows the reporting of a variety of diagnostics to evaluate the efficacy of any corrections that are applied. In particular, the R^2 of the regression equation indicates the strength of the linear relationship

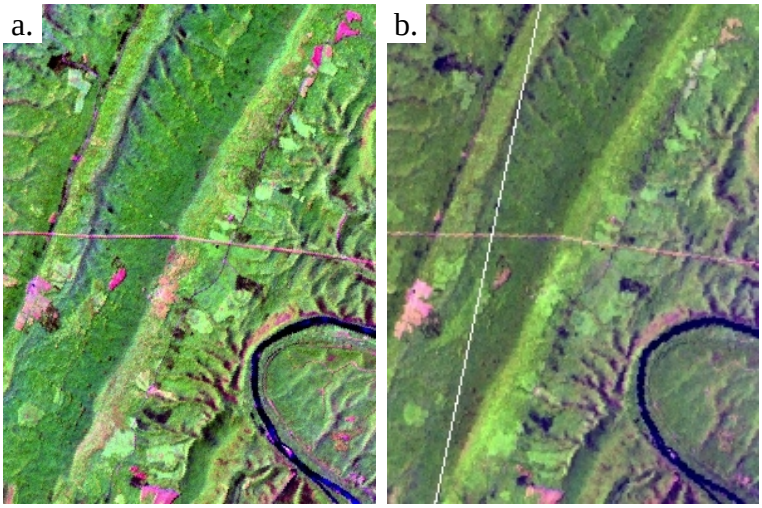

Figure 2. (a) AVIRIS image of GRSF from 14 May 2000. Bands shown in RGB are 1663 nm, 1089 nm, and 549 nm. (b) Hyperion image of the same area from 24 July 2001, showing 1659 nm, 1256 nm and 570 nm. Note the strong illumination effects along the mountain ridges.

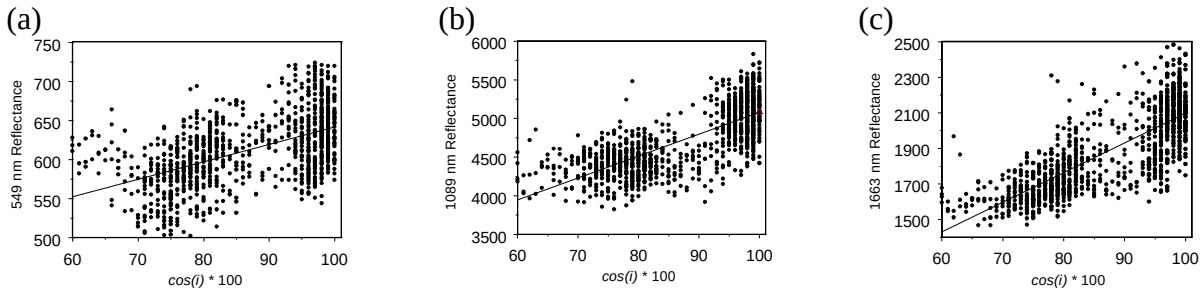

Figure 3. Relationship between illumination and reflectance for the three bands in the AVIRIS image shown in Figure 2a (14 May 2000). Values on the y-axis are 10000 * reflectance. The data shown here are for deciduous oak forests.

between reflectance and *cos(i)*. In addition, the steepness of the slope of the regression equation for any particular band denotes the relative amount of shadowing in that band, with steeper slopes indicating greater amounts of shadowing and illumination.

3. RESULTS

Regression relationships between reflectance and illumination were developed using automated routines for all bands in the AVIRIS and Hyperion images. The fit (R^2) between *cos(i)* and reflectance for all bands is shown in Figure 4. Excluding the water absorption wavelengths, most bands exhibited some relationship between *cos(i)* and reflectance (i.e., $p < 0.05$) that allowed the implementation of the normalization. For example, the R^2 for AVIRIS Band 19 (549 nm) shown on Figure 3a was 0.3; even so, implementing Equation 1 still resulted in the detrending of the data so that reflectance was no longer related to *cos(i)* (Figure 6). Most notable, however, was that the strength of the relationship between illumination and reflectance appeared to parallel the general reflectance curve for forests in GRSF. That is, the ability to correct for illumination is greater at wavelengths where the reflectance is the greatest, e.g., the near infrared where R^2 was around or above 0.6 for most bands. For example, the improved correction at the reflectance peak in the green wavelengths (558 nm) (compared to other visible bands) is especially notable on the 13 July 2001 AVIRIS image. These results are not surprising; they simply indicate that topographic effects are most readily corrected at wavelengths where the signal to the sensor is greatest. However, these results also show that robust corrections can be developed at wavelengths with low reflectance.

From a statistical perspective, an examination of R^2 only indicates how strong the relationship between illumination and reflectance is, but not the magnitude of the effect of illumination. On a band-by-band basis, the degree of terrain effect is best illustrated by examining the slope of the relationship between illumination and reflectance. That is, the greater the effect of illumination, the higher the slope between less illuminated pixels (low *cos(i)*) and more illuminated pixels (high *cos(i)*). The effects of illumination are most pronounced at those wavelengths with the highest reflectance (Figure 5). Again, this result is not surprising; it simply indicates that effects of shading are more dramatic where there is greater reflectance by the surface and hence signal strength at the sensor.

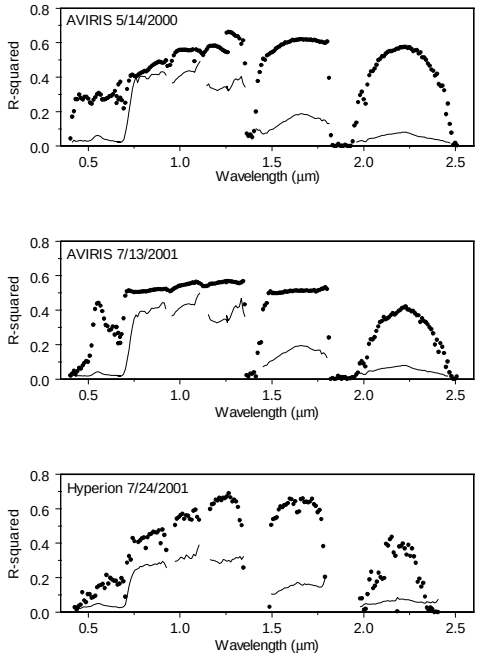

Figure 4. R^2 of reflectance as a function of illumination by wavelength (dots) for the images. Also shown is the average reflectance for oak forests in each image (lines).

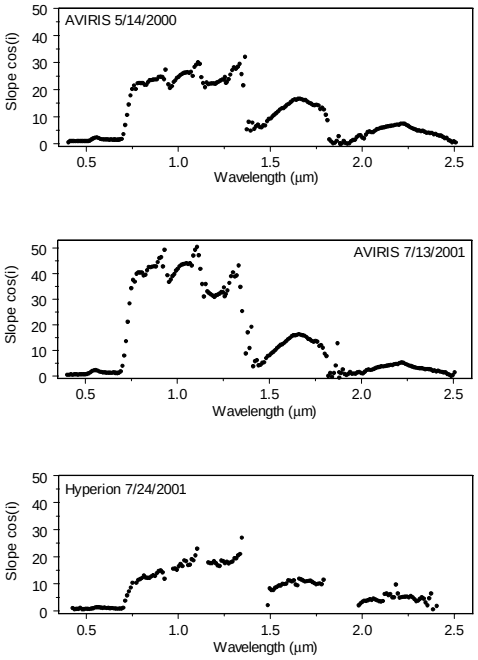

Figure 5. Slope of the regression line between reflectance and illumination by wavelength.

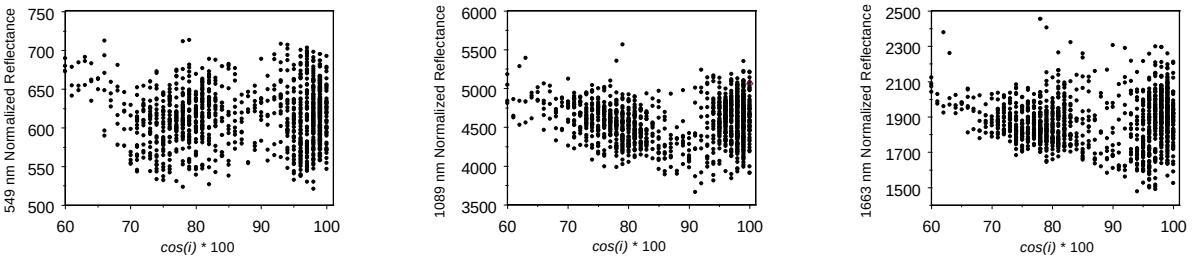

Figure 6. Relationship between illumination and reflectance following normalization for the 14 May 2000 AVIRIS image. Reflectance values on the y-axis are 10000 * reflectance.

The terrain normalization resulted in a substantial reduction of the effects of solar illumination in the AVIRIS and Hyperion images (Figures 6 and 7). In particular, areas on the illuminated and shadowed sides of steep ridges now exhibit comparable reflectance. It is notable that some areas along the ridges do not appear to have been corrected; in most cases these represent areas characterized by pines rather than oaks and as such have lower reflectance than surrounding areas. However, some areas were undercorrected, meaning that shaded slopes appear to remain shaded. These problems occur in areas where the images and DEM are slightly misregistered. An offset of even 2 pixels along the top of a steep ridge will result in a thin band of undercorrected pixels along the top of the ridge. Other DEM errors can also create problems; for example, our DEM, which was acquired from the National Elevation Database (NED), exhibited some regular striping that was corrected using a low-pass filter. However, this filtering has the effect of reducing slopes and thereby lowering apparent illumination differences as modeled from the DEM. This leads to the potential for underestimating the slope of the regression between *cos(i)* and reflectance. Nevertheless, the net effect of the correction was to reduce the effects of solar illumination, which should improve the ability to interpret the images and quantify differences in reflectance between forests with different properties.

4. CONCLUSIONS

An empirical method of terrain normalization (Allen, 2000; Meyer et al., 1993) was applied to AVIRIS and Hyperion images for a forested area of steep topography in the central Appalachian Mountains. The effects of differential illumination of the landscape were reduced in the corrected images, but were not eliminated altogether because of potential misregistration between DEMs and images. The empirical fit between reflectance and illumination was best at the near infrared wavelengths having the highest reflectance. However, statistically significant relationships between illumination and reflectance were found at almost all wavelengths. The greatest amount of correction – indicated by the steepness of the slope of the regression equation – was applied at wavelengths having highest reflectance. Therefore, we conclude that topographic effects are greatest when reflectance is highest and that those effects are also most easily modeled and corrected at the same wavelengths.

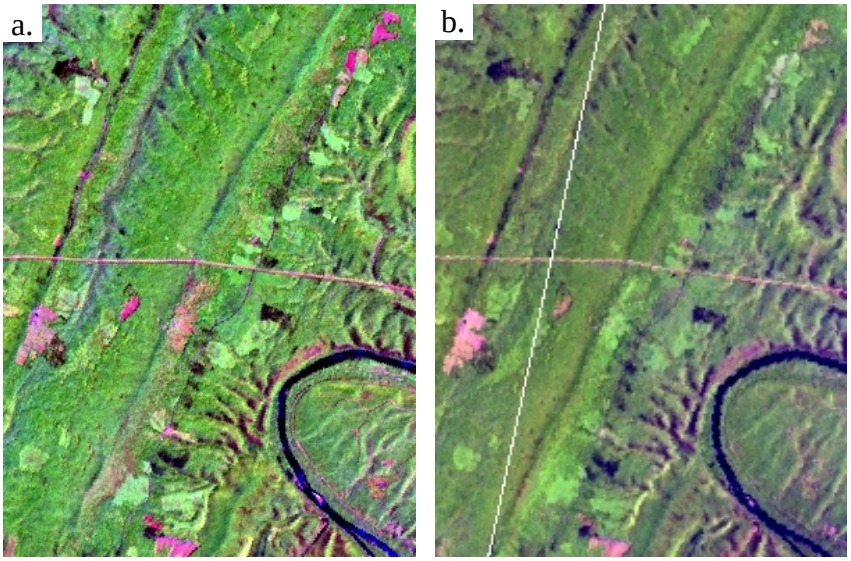

Figure 7. Normalized images of those shown in Figure 2: (a) AVIRIS from 14 May 2000 showing 1663 nm, 1089 nm, and 549 nm; (b) Hyperion from 24 July 2001, showing 1659 nm, 1256 nm and 570 nm. When compared with Figure 2, the illumination effects are greatly reduced. Dark areas on these images are generally pine forests; some areas are under-corrected due to mis-registration between the DEM and images.

Because the approach is rapid, and – with the exception of the selection of training pixels – automated, it can be readily applied to large hyperspectral data sets. Further, once training sites are established for a given area, the extraction of training data can also be automated. This approach is especially relevant for sites where the detailed information on tree physiognomy and bi-directional reflectance factors (BRDF) necessary for canopy based models are unavailable. Topographic normalization is essential for analyses of forests in rugged terrain, and the approach described here provides a simple approach with effective results.

5. ACKNOWLEDGMENTS

This research was supported by NASA EO-1 Science Validation Team grant NCC5-493. Thanks to Tom Allen for valuable discussions of terrain normalization, and to Clayton Kingdon, Carol Garner, Clay Baros and Robert Chastain for their contributions to this work. This paper is Scientific Series Contribution Number 3550-AL, University of Maryland Center for Environmental Science.

6. REFERENCES

Allen, T.R., 2000. Topographic normalization of Landsat Thematic Mapper data in three mountain environments. *Geocarto International*, 15(2): 13-19.

Civco, D.L., 1989. Topographic normalization of Landsat Thematic Mapper digital imagery. *Photogrammetric Engineering and Remote Sensing*, 55(9): 1303-1309.

Conese, C., Gilabert, M.A., Maselli, F. and Bottai, L., 1993. Topographic normalization of TM scenes through the use of an atmospheric correction method and digital terrain models. *Photogrammetric Engineering and Remote Sensing*, 59(12): 1745-1753.

Gao, B.C., Heidebrecht, K.B. and Goetz, A.F.H., 1993. Derivation of scaled surface reflectances from AVIRIS data. *Remote Sensing of Environment*, 44(2-3): 165-178.

Kennedy, R.E., Cohen, W.B. and Takao, G., 1997. Empirical methods to compensate for a view-angle-dependent brightness gradient in AVIRIS imagery. *Remote Sensing of Environment*, 62(3): 277-291.

Martin, M. E., Smith, M.L., Ollinger, S.V., Hallett, R.A., Goodale, C.L. and Aber, J.D., 1999. Applying AVIRIS at the sub-regional scale: Forest productivity and nitrogen and cation cycling. In: R.O. Green (Editor), *Proceedings of the Eighth JPL Airborne Earth Science Workshop*, Pasadena, California, pp. 275-279.

Meyer, P., Itten, K.I., Kellenberger, T., Sandmeier, S. and Sandmeier, R., 1993. Radiometric corrections of topographically induced effects on Landsat TM data in an Alpine environment. *ISPRS Journal of Photogrammetry and Remote Sensing*, 48(4): 17-28.

Minnaert, N., 1941. The reciprocity principle in lunar photometry. *Astrophysics Journal*, 93: 403-410.

Moran, M.S. et al., 2001. A refined empirical line approach for reflectance factor retrieval from Landsat-5 TM and Landsat-7 ETM+. *Remote Sensing of Environment*, 78(1-2): 71-82.